Suppressed Side-lobe, Beam Steered, C-band Circularly Polarized Array Antenna for Airborne Synthetic Aperture Radar

Mohd Zafri Baharuddin[†], Josaphat Tetuko Sri Sumantyo[†]

[†] Center for Environmental Remote Sensing, Chiba University, Japan.

***Abstract*—**A circularly polarized antenna array was designed for use with an airborne C-band synthetic aperture radar (SAR) measurement system. Designed SAR performance parameters formed the performance requirements of the array antenna. A single patch antenna was first designed to conform to the required operating frequency and axial ratio for circular polarization. This was then followed by the linear array and feed design. Several important antenna performance parameters customized for our SAR measurements were achieved in this study. Among them are low axial ratio of under 3dB with 125 MHz bandwidth via corner truncated square patches for circular polarization; steep scanning angle of 40 degrees using phased delayed 10-element array at 0.53 lambda element spacing; suppressed side-lobe level utilizing the Dolph-Chebyshev synthesis method; and reduced radiation from spurious feeds through optimized feed network using T-junctions and mitered bends. The antenna performance was estimated, followed by full electromagnetic wave simulation at each design step. The optimized design was used for fabrication of the antenna and the array antenna performance parameters was verified through measurements in an anechoic chamber. Results show agreement between theoretical and simulated data which match the design parameters. A planar array structure was also proposed to increase the total array gain.

***Keywords*—beam steering, circular polarization, Dolph-Chebyshev synthesis, patch array antenna**

I. Introduction

CIRCULARLY polarized antennas are employed in various broadcasting, communication and global positioning applications due to the advantages of insensitivity to antenna orientation, reduced multipath fading effect [1], water particle detection and weather clutter reduction [2]. Al-Jumilya et.al and Okamura et.al both studied circularly polarized electromagnetic wave polarization effects of rain. They concluded that rain or hail detection can be increased or decreased according to receive-transmit polarization pairs [3], [4]. An application of circularly polarized (CP) antennas that is just gaining ground is in synthetic aperture radar (SAR). Typical SAR systems utilize linearly polarized antennas such as DLR's spaceborne TerraSAR-X satellite [5], NASA's airborne UAVSAR [6], and ONERA's Airborne Multi- Frequency SAR Imaging Systems [7]. Full polarimetric imaging analysis has been extensively studied for spaceborne and airborne that use linearly polarized measurements. Compact SAR is a mode where the system receiver is linearly polarized but the transmitter is circularly polarized [8]. The Japanese Aerospace Agency (JAXA) has an experimental compact SAR mode on their ALOS-2 earth observation satellite [9]. Several SAR systems have begun attempts to use CP antennas for both receive and transmit [10]. All these CP antennas have radiation patterns with main lobes in the direction normal to the antenna. This means that the antenna has to be rotated and pointed towards the target of interest.

Proper care is required in the antenna design process to ensure that the integrated system functions optimally. Table 1 compares antenna parameters of several airborne SAR systems. To scan at a desired look angle, the antenna can simply mounted at an angle [11]. Flexible beam steering can be achieved by using digital beamforming [12]. This steep beam steer is difficult to achieve using just constrained feeding, without digital beamforming. As demonstrated by [13] and [14] a beam steered antenna simplifies planar mounting on an aerial platform.

Parameter.	*NASA DB-SAR*	*DLR F-SAR*	*MMU UAVSAR*	*Proposed SAR*
Polarization	Linear	Linear	Linear	Circular
Frequency	1.26 GHz	5.3 GHz	5.3 GHz	5.3 GHz
Bandwidth	20 MHz	400 MHz	80 MHz	125 MHz
Antenna type	Planar microstrip patch array			
Signal to noise ratio	-18 dB	-20 dB	-15 dB	-15 dB
Antenna size	1.2 x 1.0 m	0.96 x 0.5 m	1.0 x 0.3 m	0.8 x 0.3 m
Pulse power	350 W	700 W	50 W	50 W
Antenna beam steer	±45°	0°	25°	40°
Steer method	Digital	Fixed	Fixed	Fixed
Flight platform	P-3 Orion	Dornier DO228-212	Aludra MK1 UAV	Boeing 737-200

Table1 Comparison of notable airborne SAR systems.

Considering the above, our lab has embarked on a project to develop an airborne SAR system that utilizes CP radiating signals for transmission, detection and processing. Among the research planned to be conducted with our SAR system is mapping of land surface, interferometry and wave scattering mechanism of snow or ice, vegetation, rocks and desert areas. Potential applied research includes ocean monitoring, snow or ice monitoring and disaster monitoring.

In this paper, a circularly polarized antenna array employing a steep 40 degree beam steer as well as side-lobe reduction using the Dolph-Chebyshev synthesis method at C-band 5.3 GHz is presented. Section II of this paper will discuss the radiation pattern design considerations and antenna performance requirements by the SAR system. Section III explains the design process of the proposed array antenna. Performance characteristics of the simulated and fabricated antennas were compared and shown in Section IV.

II. Radiation Pattern Design Considerations

The antenna developed in this work is to be used in an airborne SAR system. Comparatively to spaceborne systems, airborne SAR operates at a much lower altitude and thus has a different set of operating parameters such as shorter range, and a lower average transmit power. In our case the SAR range is around 15 km with an average transmit power of 50 watts based on a previous study [15]. The travelling speed is also much slower thus the pulse repetition frequency (PRF) requirement is lower.

The initial study provided the antenna performance requirements as a starting guideline. The SAR system is to be operated on a Boeing 737-200 aircraft with the antenna mounted on a location above the fuselage, between the front wings and rear stabilizers as shown in . To reduce power loss it is desired that the transmission line lengths be minimized. As such, the SAR system processor and data logging are installed in a working compartment at the rear of the aircraft fuselage, while the RF front-end (transceiver module) is located in the radome with the antenna. Connection between the RF front-end and the antennas is made with minimal use of semi-rigid cables.

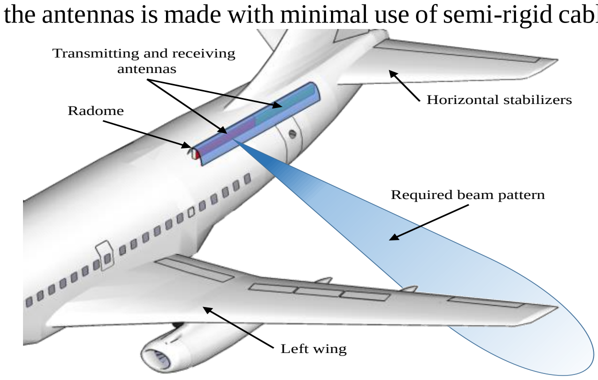

Figure 1 Location of antennas and required beam pattern path.

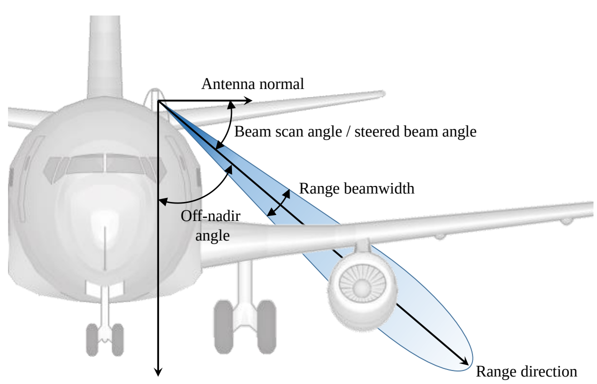

Figure 2 Profile of desired antenna beam pattern.

Corresponding author:
Mohd Zafri Baharuddin (email: mdzafri@gmail.com)

Only a few works have treated visibility analysis in urban

The radiation pattern design of the SAR antenna depends on factors such as azimuth ambiguity, range ambiguity, and reflections from the aircraft structure [13]. For acceptable performance an azimuth ambiguity over signal ratio (AASR) and side-lobe level (SLL) of -20 dB was derived. Range ambiguity is caused by scattering received from earlier or later pulses arriving back to the antenna at the same time as the desired echo. Proper design of the antenna fixture and suppression of the side-lobes can significantly reduce unwanted signal reflections on the aircraft structure.

Taking into account the SAR design constraints above and the vertical mounting orientation of the antenna shown in, the vertical and horizontal plane radiation patterns were designed. For the vertical plane a 3-dB beam-width of 11 degrees and a beam steer angle of 40 degrees from the antenna normal is required. In the horizontal plane a beam-width of 5 degrees with no beam steer was specified. The total circular polarization gain of the array should be at least 17 dBiC.

For full polarimetric measurements a total of four antennas will be required; two left hand-polarized and two right-hand polarized. As an operational example, if a left-handed antenna is transmitting, a different left-handed antenna and a right-handed antenna will receive the backscattered signal. The receiving-transmitting pair notations are listed in Table 2. The antennas are marked on the right side of the RF system diagram in Figure 3. Each back-scattered radar signal is digitized in the real and imaginary format, and saved for SAR image generation during post processing.

Receive	*Transmit*	*Notation*
Left	Left	LL
Right	Right	RR
Right	Left	RL
Left	Right	LR

Table2 Circular polarization (left/right-handed) notation for receive and transmit antennas.

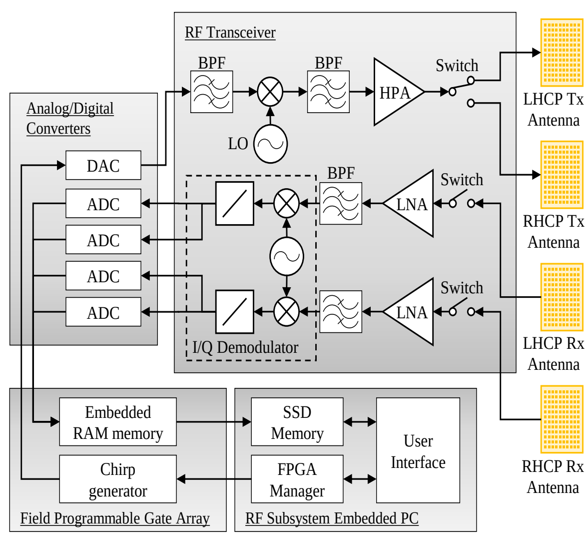

Figure 3 Profile of desired antenna beam pattern.

III. Problem Design of Microchip Patch Antenna

The radiation pattern requirements can be achieved with a planar microstrip patch array. The patch array design process begins with designing a single patch element to comply with the operating frequency and circular polarization performance requirements. The single element patch was repeated multiple times in a row with uniform spacing to form a linear array. Antenna synthesis was performed to reduce side-lobe levels typically generated by uniform arrays. To conform to the look angle of the SAR system, a 40 degree scanning angle was applied. Finally, with the designed parameters, the feed network consisting of power splitters/combiners and transformers was designed. Each step of the array design is explained in further detail in the following subsections. Ten elements were used to generate the vertical plane pattern, whilst 12 elements were required for the horizontal-plane, resulting in a 120-element array.

A. Single element design

An electromagnetically coupled square patch was used as the radiating element because a wider impedance bandwidth is desired. The structure contains two substrates with the same dielectric constant. The radiating patch is on the top, the feed line in between the two substrates, and the ground layer is at the bottom. With this structure spurious radiation was also reduced as the feed line is located closer to the ground plane. A combined thicker substrate between the radiating patch and ground plane also provides improved impedance bandwidth over the conventional microstrip-fed patch [16], [17].

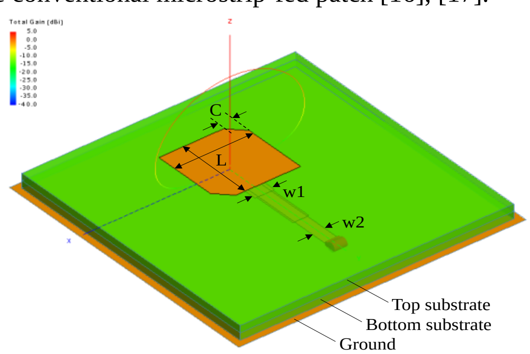

Figure 4 Single element corner truncated patch antenna on dual substrates. Also shown is the radiation pattern that peaks at 5.0-dBiC at the boresight.

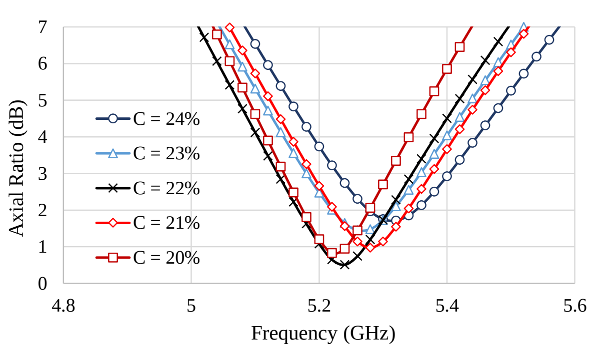

Figure 5 Figure 5: Axial ratio values as a function of the truncation size. The truncation size is shown as a percentage of the patch width.

Geometry design of the single patch is presented in Figure 4. Two identical layers of Nippon Pillar substrate was used, each with 1.6 mm thickness, relative permittivity of 2.85 and loss tangent of 0.0024. Patch dimensions of 15.54×15.54mm results in a center operating frequency of 5.3GHz. The feed line, w2, has a width of 2.533 mm for an impedance of 50Ω and a length of 26.813mm or 3λ/4 to have the current peak at the radiator. The feed width under the radiator, w1, is 3.822 mm for an impedance of 39.95Ω. We used a quarter-wave transformer to match the impedances of the single patch feed.

For circular polarization, truncations were made at two opposing corners to excite the two orthogonal modes simultaneously with a 90 degree time-phase difference. Axial ratio was calculated as a measure of circular polarization. As shown in Figure 5, varying the truncation length changes the axial ratio value. Axial ratio values under 3dB is considered to be circularly polarized. Optimizing the length to 22% of the patch length, the axial ratio was minimized.

B. Steered beam design

Based on the design requirements, the antenna main beam needs to be steered to a steep angle of 40 degrees due to the vertical mounting of the antenna on the aircraft. Since in our implementation there is no need for digital beamforming, we adopted a phased-shifted linear array structure. In this structure the beam steer angle is fixed.

The phase increment, $\Delta\varphi$, between each successive element was calculated using equation (1), where d is the distance between the individual patches, Θ_s is the steer angle, and lambda is the system wavelength [18].

$$\Delta\varphi = \frac{360^\circ \cdot d \cdot \sin\Theta_s}{\lambda} \tag{1}$$

The value of d cannot be too large to avoid unwanted grating lobes. The value of d was selected to be 0.53λ. The steering angle also has a limit. Steering to an angle that is too steep can result in increased side-lobe level, reduced gain and degraded performance. We performed a parametric study to find this limit, with results presented in Section IV. The calculated phase delay for each patch element is shown in Table 3. Phase delays were implemented using carefully sized microstrip lines which will be explained in Section III-D.

Element	1	2	3	4	5	6	7	8	9	10
Relative amplitude	0.045	0.069	0.103	0.133	0.150	0.150	0.133	0.103	0.069	0.045
Phase (degree)	0	135	270	405	540	675	810	945	1080	1215
Phase (lambda)	0	0.375	0.750	1.125	1.50	1.875	2.250	2.625	3.00	3.375
Distance from feed (mm)	117.4	130.2	143.0	155.8	168.6	181.4	194.2	207.0	219.8	232.6

Table2 Derived excitation coefficients and phase delay for each patch element.

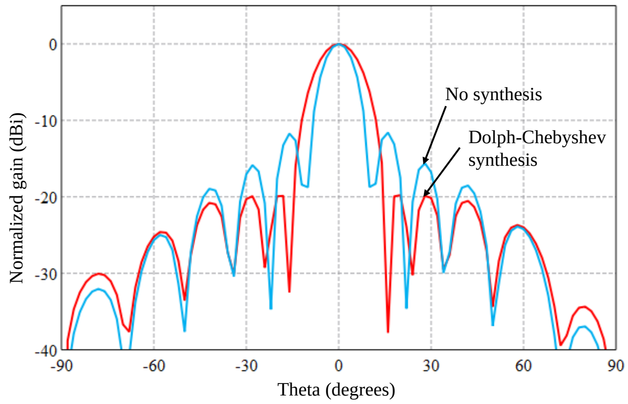

Figure 6 Comparison of a 10-element radiation pattern with and without the proposed synthesis method

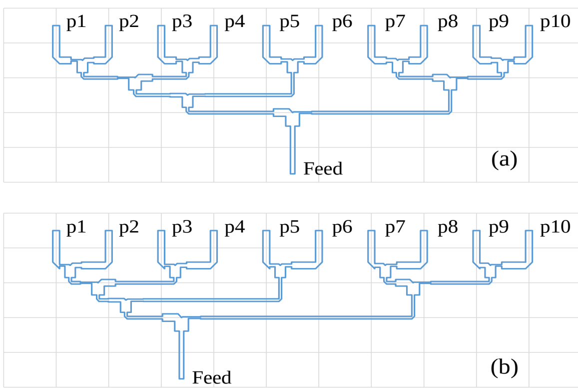

Figure 7 Design of microstrip feed network with synthesized power distribution: (a) Zero degree beam steer; (b) 40-degree beam steer. Note the shifted lengths of the microstrip lines.

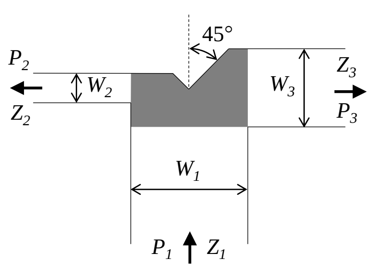

Figure 8 Unsymmetrical microstrip T-junction design.

C. *Design of reduced side-lobe*

Our perception models are based on physical models A linear array with uniform power division typically results in good gain in the main lobe, but also large side-lobe levels which can add to cross-range ambiguity in the SAR processing. To further reduce the signal-to-noise ambiguity, the radiation pattern side-lobes were reduced by utilizing the Dolph-Chebyshev synthesis method to find the array factor for each element. The array consists of 10 elements arranged linearly with equal spacing, d, between each element. Based on AASR requirement and system PRF, a side-lobe level of -20dB would provide sufficient AASR for good SAR system performance. This value was used as input to the Dolph-Chebyshev synthesis using the array factor equation below [16].

$$(AF)_{2N} = \sum_{n=1}^{N=5} w_n \cos\left[(2n-1)u\right] \quad (2)$$

$$u = \frac{\pi d}{\lambda}\cos\theta \quad (3)$$

Where w_n is the excitation coefficients of each array element. Solving the above equations with the cosine series expansion, the array factor equation becomes:

$$(AF)_{10} = 0.15\cos u + 0.133\cos 3u$$
$$+ 0.103\cos 5u + 0.069\cos 7u + 0.045\cos 9u \quad (4)$$

The synthesis output for each antenna element is shown as array excitation coefficients in Table 3. As a comparison, Figure 6 shows the simulated radiation patterns of the designed array with and without the synthesized array factors. Note the drop in side-lobe magnitude as well as expansion of the beam-width compared to the un-synthesized radiation pattern. The reduction of the side-lobe is important for improving range and cross-range ambiguity during image construction of the synthetic aperture radar.

D. *Array Signal Distribution Network*

The Once the phased shift angle and array factors have been derived, these values can be used to design the array signal distribution network. The distribution network will channel energy to each patch at the right time and magnitude to generate the designed beam pattern. A corporate feed network was utilized with lengths kept short and line widths narrow to minimize spurious radiation [17]. The network has an input impedance of 50Ω while most of the microstrip line has an impedance of 67Ω.

To implement the steered beam of Section III.B, the phased shifted network was designed by delaying the signal to each subsequent element. The simplest way to achieve this is to increase the distance travelled by the signal. This method of delayed power feed is a form of constrained feeding. Each patch will be fed with a signal that is delayed by a phase of $\Delta\varphi$ degrees, or a length of d_φ, as calculated from:

$$d_\varphi = \frac{\Delta\varphi}{360°} \times d_\lambda \quad (5)$$

Where d_λ is the electrical length the microstrip line at the center operating frequency when using the specified substrates. This electrical length can be estimated through calculations but it was found that EM simulation results provided values closer to the actual length.

With the calculated feed delay lengths for each element, the feed network for beam steering was designed as shown in Figure 7(b). As compared to the feed network with no phase delay in Figure 7 (a), the phase delayed network has a feed microstrip lines that are shifted to one side. This will affect the radiation beam pattern slightly.

To implement the reduced side-lobe of Section III.C, unsymmetrical microstrip T-junction power dividers [19] were used in the feed network to divide the power to each patch according to the calculated array factors. Figure 8 shows a modified unsymmetrical T-junction with a v-notch to improve power division. Each T-junction was sized specifically using (6) to match the final output requirement at the individual patches.

$$Z_1 = \frac{Z_2 \times Z_3}{Z_2 + Z_3}, \; P_2 = \left(\frac{Z_1}{Z_2}\right)P_1, \; P_3 = \left(\frac{Z_1}{Z_3}\right)P_1 \quad (6)$$

The calculated impedances, Zn, for each power divider would have a specific line width, Wn, when implemented as an embedded microstrip. The respective line widths can be calculated by solving for W in the following equations:

$$Z = \frac{60}{\sqrt{\varepsilon_e}} \ln\left(\frac{5.98h}{0.8W + t}\right) \quad (7)$$

$$\varepsilon_e = \varepsilon_r \left(1 - \exp\left(-1.55\frac{h_1}{h}\right)\right) \quad (8)$$

Where h is the dielectric thickness, h_1 is the total thickness of both substrates, t is the trace thickness, ε_r is the relative dielectric constant, ε_e is the effective dielectric constant, and Z is the required impedance.

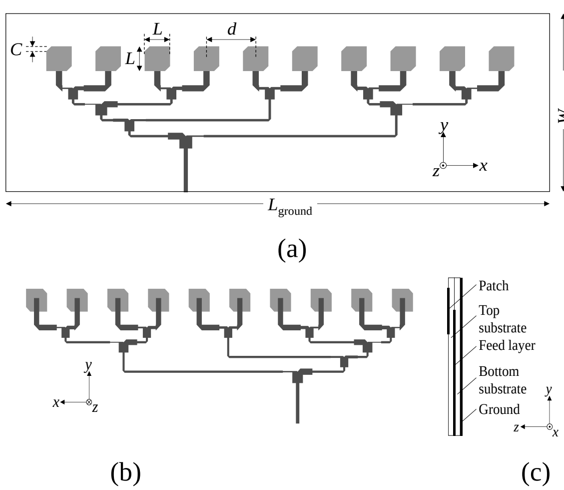

Figure 9 Geometry of left-handed circularly polarized array antenna: (a) top view (light gray is radiating patch, dark gray is the feed network); (b) bottom view; and (c) side view.

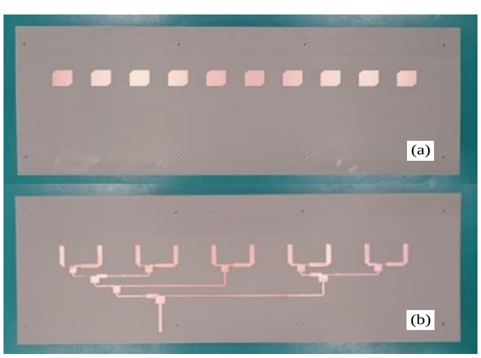

Figure 10 Prototyped left-handed circularly polarized array antenna: (a) top substrate; (b) bottom substrate.

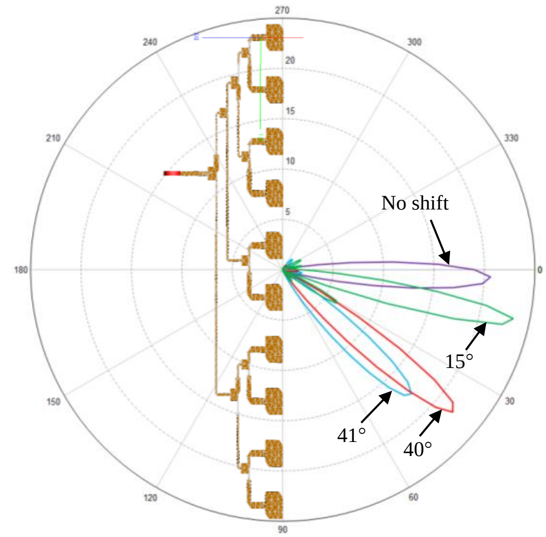

Figure 11 Magnitude and beam steering at different angles. 40 degrees provides the best compromise of steer angle and gain.

IV. Simulation and Measured Results

The proposed 10×1 element array antenna was studied using the FEKO electromagnetic simulation software. The simulation process starts with designing a balanced feed with no delay lines and uniform power distribution. The scattering parameters at the output to each element was observed to confirm that the feed has equal phase and power. Next, feed lines were introduced to apply beam steering, followed by unsymmetrical T-junction power dividers. The scattering parameters were observed and confirmed at each step, making adjustments to the calculated input if necessary. To complete the 10×1 element array, the optimized radiating patch was applied. The full model was then simulated for return loss, axial ratio, input impedance, and far field radiation patterns. Using the finalized design, the beam steered, synthesized 10×1 element array was fabricated and a left-handed CP prototype is shown in Figure 10. The fabricated array antenna performance parameters were then measured to confirm agreement with the simulated results.

A. Beam steered, synthesized 10×1 array

Beam steering at varying angles were studied to determine the maximum angle possible with the designed feed network. Figure 11 is a polar diagram showing the radiation pattern magnitudes of several notable angles. As expected, the main lobe is in the +z-direction when no steer was implemented. It is interesting to note that the gain increases slightly when the beam was steered above 15 degrees. The raised gain was maintained until around 40 degrees, after which there is a sharp decline in gain. This was due to the appearance of grating lobes on the opposite side of the array. Magnitudes of other side-lobes also increase above 40 degrees. At beam steer angles larger than 41 degrees, the T-junctions closest to the first element will not have enough space and a total redesign of the feed will be required. As such the maximum beam steer angle limit is 40 degrees.

Once the desired beam steer was achieved, a full 3D radiation pattern was simulated to ensure no excessive spurious radiations occur. The simulated 3D radiation pattern in decibel and magnitude scales are shown in Figure 12. The side-lobe in the +z-direction is the largest and several side-lobes were found to be slightly above the designed –20dB side-lobe level requirement.

After optimization in the software, we fabricated the designed array antenna in-house using chemical etching. Both radiating patch and feed network layers of the fabricated antenna are shown separately in Figure 10. Scattering parameters were taken using a vector network analyzer and far field radiation patterns were measured in the Josaphat Microwave Remote Sensing Laboratory (JMRSL) anechoic chamber facility.

The measured and simulated return losses of the proposed array antenna in Figure 13 show good agreement. The realized bandwidth is 215 MHz (4.1%) from 5.157 GHz to 5.39 GHz at a center frequency of 5.2825 GHz, which matches the 215 MHz (4.0%) simulated bandwidth but at a slightly different frequency range from 5.165 GHz to 5.38 GHz with a center frequency of 5.2725 GHz.

A far field frequency sweep was measured between the proposed antenna and a set of left and right-handed CP spiral cone antennas to calculate the gain and axial ratio. Angle of measurement had to be properly planned as the beam steering must be taken into account. An axial ratio of 125MHz or 2.43% (5.085–5.210GHz) seen in Figure 14 was measured at the 40 degree boresight angle. Simulated axial ratio was slightly less at 120 MHz or 2.30% (5.155–5.275GHz). The measured gain plot must be compared to an isotropic antenna gain to calculate the realized gain [20]. A 5.3 GHz dipole antenna was measured and its peak gain was used as the isotropic gain value. The realized left-handed gain was calculated and the graph has some agreement with the simulated results as also shown in Figure 14. The peak left-handed CP gain was measured at 12.1 dBiC, slightly lower than the simulated gain of 12.7 dBiC. The differences between simulated and measured values can be attributed to manufacturing imperfections.

Lastly, an angular sweep was performed to obtain the array radiation pattern at the designed operating frequency of 5.3GHz. The proposed antenna was placed on a rotary turntable and measured in the far field with standardized CP antennas. The measured and simulated left-handed radiation patterns are shown together in Figure 15. Simulation was performed on an infinite substrate, thus there is no radiation below the ground layer as shown by the dotted line plot. There was good agreement between the radiating sides of the two plots. However in terms of side-lobe performance, and as noted before, the side-lobe levels did not conform to the -20dB requirement. The measured radiation pattern shows a side-lobe level of -15dB which is still an improvement of over 5dB compared to an un-synthesized feed network. The beam steer was successfully implemented as the main lobe is clearly directed in the 40 degree direction, with a half-power (3-dB) beam-width of 11.5 degrees.

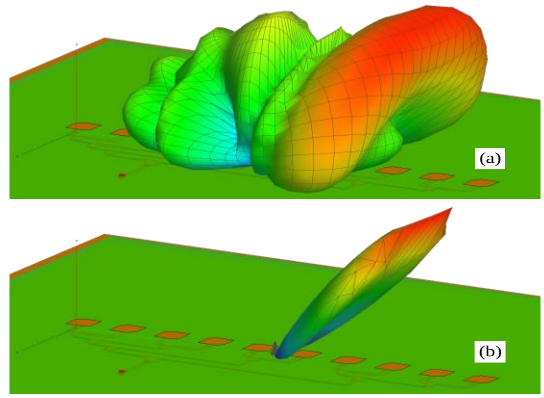

Figure 12 Simulated 3D radiation pattern at 40 degree beam steer: (a) decibel scale; (b) magnitude scale.

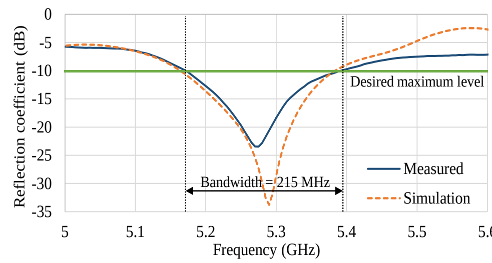

Figure 13 Measured and simulated return losses of the proposed array antenna.

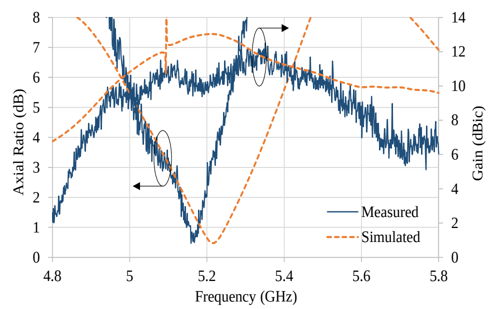

Figure 14 Measured and simulated axial ratio of the proposed array antenna.

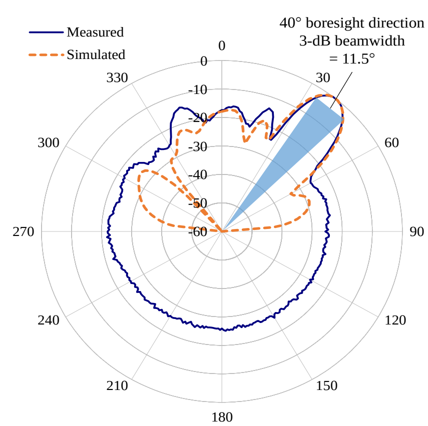

Figure 15 Measured and simulated radiation pattern of the designed left-handed circularly polarized array. Simulated maximum gain was 12.7 dBiC, measured gain was 12.1 dBiC.

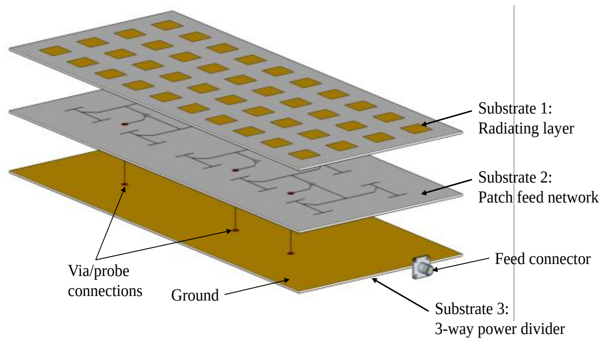

Figure 16 Proposed array module structure. From top: radiating patch, feed network, and 3-way power divider layers.

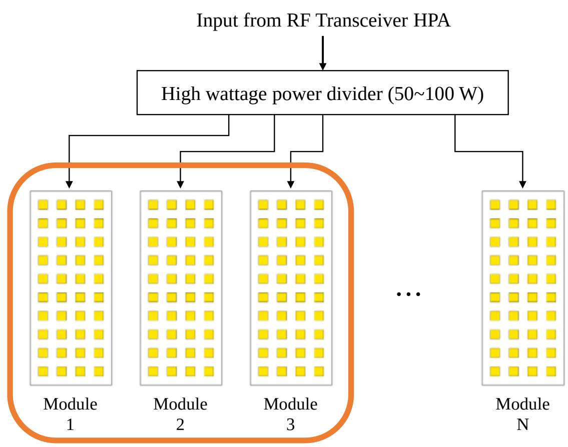

Figure 17 With a high wattage power divider, use of multiple modules can increase the total system gain as required.

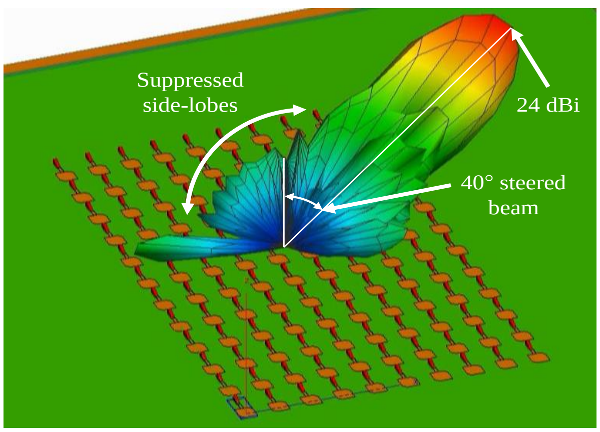

Figure 18 Simulated 3D radiation pattern of a 10×12 element array achieved by utilizing three antenna modules.

B. Array module to achieve target gain

A study into the design of a suppressed side-lobe, beam-steered, CP 10×1 element array antenna was completed. The design procedures resulted in a fabricated antenna that matches with simulation results. However, the single linear array with 10×1 elements was not sufficient to generate the required minimum gain of 17 dBiC. To reach this requirement, a larger planar array has to be designed. A modular structure was adopted for ease of mounting, transport and increasing the gain if required.

Figure 16 presents the proposed three layer substrate array module structure. The radiating patches in the top substrate is the same as designed in this paper. The feed network of the middle layer will also contain the designed phase delays and power distribution for steered beam and reduced side-lobes. The additional layer at the bottom will have via probes connecting to an unbalanced 3-way Wilkinson power divider. This power divider will perform the same function as the first stage divider of the linear array design, but with greater efficiency. Each module would contain 10×4 elements to generate 18 to 19 dBiC of gain which complies with the minimum system gain requirement.

If higher gains are required, additional modules can be added. For example as shown in Figure 17, three modules can achieve a gain between 21-24 dBiC. Figure 18 shows the radiation pattern generated by a 10×12 element array consisting of three of the proposed modules for a total of 120-elements. The boresight was still steered by 40 degrees and side-lobes were suppressed to between -15 dB and -20 dB. The vertical plane 3-dB beam-width was 11.5 degrees, the same as the 10×1 array. Meanwhile, the horizontal plane 3-dB beam-width was 5 degrees.

V. CONCLUSION

A simple corner truncated square patch was used as elements in a beam steered array. By using a corporate feed structure with unsymmetrical T-junction power dividers and varying feed line lengths, a side-lobe level of -15 dB and steep beam steer angle of 40 degrees was achieved. The power to each patch was distributed using a Dolph-Chebyshev synthesis to reduce the side-lobe levels. After simulation and optimization, the designed 10-element array was fabricated. The fabricated prototype achieved a circular polarized bandwidth of 125 MHz or 2.43% (5.085 – 5.210 GHz) and impedance bandwidth of 215 MHz or 4.1% (5.157 – 5.39 GHz). An antenna peak gain of 12.1 dBiC was realized with a half-power beam-width of 11.5 degrees. With the achieved performance parameters of the prototype, a set of the proposed array antenna is suitable for use as transmit and receive antennas in the planned airborne circularly polarized synthetic aperture radar system. To increase the gain, we proposed a planar array structure with simulated results showing compliance depending on the SAR system gain requirements. The modular structure makes it easier to customize the antenna size to different missions.

ACKNOWLEDGEMENT

This work was supported by the Japanese Ministry of Education, Culture, Sports, Science and Technology (MEXT), and the Japan International Cooperation Agency (JICA). The authors would like to thank their kind sponsors.

REFERENCES

[1] F. Yildirim, A. S. Sadri and H. Liu, “Polarization Effects for Indoor Wireless Communications at 60 GHz,” in IEEE Communications Letters, vol. 12, no. 9, pp. 660-662, September 2008.

[2] Kais J. Al-Jumily, Robert B. Charlton, and Robert G. Humphries, “Identification of Rain and Hail with Circular Polarization Radar,” in J. Appl. Meteor., 30, 1075–1087, 1991.

[3] S. Okamura, and T. Oguchi, “Electromagnetic Wave Propagation in Rain and Polarization Effects,” Proceedings of the Japan Academy, Series B, Physical and Biological Sciences 86.6: 539–562, 2010.

[4] Paul A. Lynn, *Radar Systems*, Springer, pg. 76, 1987.

[5] M. Stangl, R. Werninghaus and R. Zahn, "The TERRASAR-X active phased array antenna," Phased Array Systems and Technology, IEEE International Symposium on, pp. 70-75, 2003.

[6] Yunling Lou, Scott Hensley, Roger Chao, Elaine Chapin, Brandon Heavy, Cathleen Jones, Timoth Miller, Chris Naftel, and David Fratello, “UAVSAR Instrument: Current Operations and Planned Upgrades,” Earth Science Technology Forum, Pasadena, CA: Jet Propulsion Laboratory, National Aeronautics and Space Administration, June 21, 2011.

[7] O. Ruault du Plessis and P. Dreuillet, "The ONERA airborne multi-frequency SAR imaging systems," Radar, 2013 International Conference on, Adelaide, SA, pp. 85-90, 2013.

[8] R. K. Raney, "Hybrid-Polarity SAR Architecture," in IEEE Transactions on Geoscience and Remote Sensing, vol. 45, no. 11, pp. 3397-3404, Nov. 2007.

[9] Yukihiro Kankaku, Yuji Osawa, Shinichi Suzuki, and Tomohiro Watanabe, “The Overview of the L-band SAR Onboard ALOS-2,” Progress In Electromagnetics Research Symposium Proceedings, Moscow, Russia, August 18-21, 2009.

[10] J. T. Sri Sumantyo, "Development of circularly polarized Synthetic Aperture Radar onboard Unmanned Aerial Vehicle (CP-SAR UAV)," Geoscience and Remote Sensing Symposium (IGARSS), 2012 IEEE International, Munich, pp. 4762-4765, 2012.

[11] R. Horn, A. Nottensteiner, A. Reigber, J. Fischer, and R. Scheiber, "F-SAR — DLR's new multifrequency polarimetric airborne SAR," IEEE International Geoscience & Remote Sensing Symposium, South Africa, 2009.

[12] R. F. Rincon, M. Perrine, M. McLinden, and S. Valett, “Digital Beamforming Synthetic Aperture Radar (DBSAR) Polarimetric Upgrade,” ESTF 2011 (Earth Science Technology Forum 2011), Pasadena, CA, USA, June 21-23, 2011.

[13] P. N. Tan, T. S. Lim, V. Gobi, and Y. K. Chan, “Design and development of a dual operating mode microstrip patch antenna for unmanned aerial vehicle synthetic aperture radar,” Progress In Electromagnetics Research C, Vol. 27, 143-156, 2012.

[14] N. Chamberlain, M. Zawadzki, G. Sadowy, E. Oakes, K. Brown and R. Hodges, "The UAVSAR phased array aperture," 2006 IEEE Aerospace Conference, Big Sky, MT, 2006.

[15] H. Saito, and J.T Sri Sumantyo, “Synthetic Aperture Radar for UAVs and Small Satellites,” IEICE Trans. on Comm., Vol. J97-B No.11, pp.992-998, 2014.

[16] C.A. Balanis, *Antenna Theory*, 3rd ed. Hoboken, N.J.: Wiley, 2005.

[17] J.F. Zurcher, and F.E. Gardiol, *Broadband Patch Antennas*, Norwood, M.A., Artech House: 1995.

[18] C. Wolff (2016, April 12). *Phased Array Antenna* [Online], Available: http://www.radartutorial.eu/06.antennas/Phased%20Array%20Antenna.en.html

[19] E. Hammerstad, “Computer-Aided Design of Microstrip Couplers with Accurate Discontinuity Models,” Symposium on Microwave Theory and Techniques, pp. 54-56, June 1981.

[20] IEEE Standard Test Procedures for Antennas, in ANSI/IEEE Std 149-1979, 1979.